Performance Evaluation of RAKE Receiver for Low Data Rate UWB Systems using Multipath Channels for Industrial Environments

Muhammad Gufran Khan, Jörgen Nordberg

May 26, 2008

Abstract

Since US FCC passed a resolution in 2002 allowing ultra wideband (UWB) transmissions within a specified unlicensed spectral mask, the interest in UWB technology has grown tremendously. The large bandwidth, low power spectral density (PSD), high multiple access capability and high resolution are some qualities of UWB technology. For UWB communication systems, the industrial environments are an important scenario. However, due to large number of metallic scatterers in the environment, the multipath offered by UWB channels is dense and many multipath components have significant energy. In this report, the performance evaluation of RAKE receivers for a single user system operating in non-line-of-sight (NLOS) scenarios in industrial environments is presented. The channels used for the evaluation are measured in a medium-sized industrial environment. In addition, the standard IEEE 802.15.4a channel model for NLOS industrial environment is used for comparison with the results of the measured channels. The performance is compared for partial RAKE (PRake) and selective RAKE (SRake) in terms of uncoded bit-error-rate (BER) with the assumption that the channel is known. The effect of different number of fingers on BER of PRake and SRake is studied. Moreover, the performance of maximal ratio combining (MRC) and equal gain combining (EGC) is compared for PRake and SRake receiver. The results also provide a performance comparison between different Tx-Rx separations. Finally, based on the simulation results, conclusions are presented considering the performance and complexity issues.

Chapter 1

Introduction

1.1 Overview of UWB

Ultra-wideband (UWB) radio is emerging worldwide as a particularly appealing transmission technique for applications requiring either high bit rates over short ranges or low bit rates over medium-to-long ranges [1]. The UWB technology offers some unique qualities such as wide unlicensed bandwidth, low power spectral density, high multipath resolution and multiple access capability, which make these systems an attractive choice for different applications. The history of UWB technology, conventionally called 'impulse radio' (IR), roots back to 1960's when US military used nanosecond pulses for covert communications and radar. Beginning in the late 1980's, small companies specializing in UWB started basic research and development on communications and positioning systems [2]. In April 2002, after extensive commentary from industry, the FCC issued its first report and order on UWB technology [3], thereby providing regulations to support deployment of UWB radio systems [2]. The FCC regulations classify UWB applications into several categories with different emission regulations in each case [2]. The spectral mask assigned by FCC for indoor UWB communication systems is shown in Fig. 1.1.

UWB characterizes transmission systems with instantaneous spectral occupancy of 500 MHz or a fractional bandwidth of more than 20% [4]. The fractional bandwidth is defined as [4]

$$f_{BW} = \frac{f_H - f_L}{f_c}, \tag{1.1}$$

where $f_c = (f_H + f_L)/2$ with f_H being the upper frequency of the -10 dB emission point, and f_L the lower frequency of the -10 dB emission point,

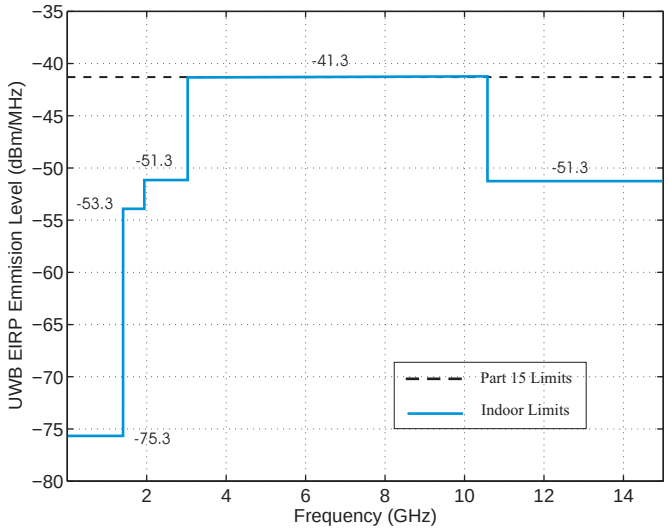

Figure 1.1: FCC allocated spectral mask for indoor ultra wideband communication systems [3].

as shown in Fig. 1.2. This definition employs that UWB is not a specific technology anymore, it is an available license-free spectrum.

The IR-UWB systems use short subnanosecond pulses that occupy a very wide frequency spectrum. The channel capacity C (in bits per second (bps)) of the band-limited additive white Gaussian noise (AWGN) channel increases with RF bandwidth [2]:

$$C = B_{RF} \log_2(1 + \frac{P_{rec}}{B_{RF} N_o}), \tag{1.2}$$

where B_{RF} is the RF bandwidth of the channel and P_{rec} is the received signal power and N_o is the noise power spectral density (PSD) in the RF bandwidth of the radio. This equation is based on an idealized rectangular filter of width B_{RF} and does not account for many effects in real systems, including interference of all sorts, receiver mismatch, and so forth [2].

The applications of UWB can be broadly divided into two categories depending on the data rates. A wireless personal area network (WPAN) is a short-range (10-15 m) high data rate wireless communications system. According to IEEE 802.15.3a standardization group, UWB technology is a promising physical layer candidate for WPANs. The applications of UWB with relatively low data rates include e.g., sensor networks, wireless body area network(WBAN), imaging, ranging and radar [5].

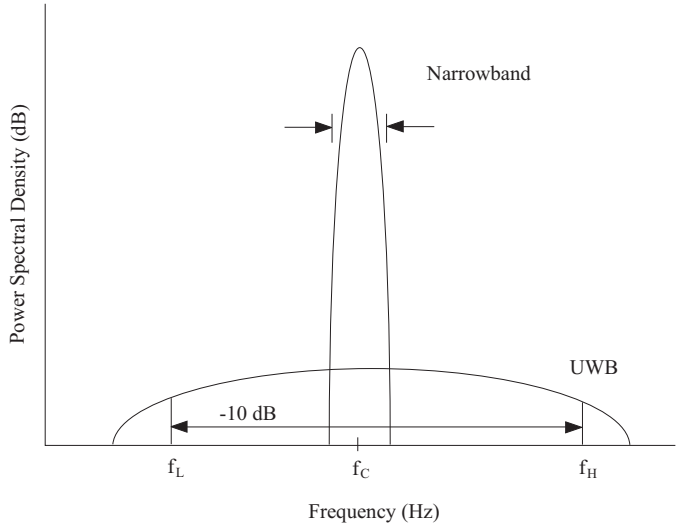

Figure 1.2: Comparison of the Fractional bandwidth of a narrowband and ultra wideband communication system [6].

1.2 Types of UWB System

There are two common forms of UWB: one based on sending very short duration pulses to convey information called Impulse Radio UWB (IR-UWB) and another approach using multiple simultaneous carriers called Multicarrier UWB (MC-UWB) [6].

1.2.1 IR-UWB System

The concept of IR-UWB is to transmit the information using a train of pulses, either with pulse position modulation (PPM), pulse amplitude modulation (PAM) or binary antipodal modulation. Typically, each symbol consists of multiple frames carrying one pulse per frame. Multiple pulses are associated with a single symbol to obtain sufficient energy per symbol while maintaining sufficiently low PSD [6].

Generally adopted pulse shapes for UWB communications include the Gaussian pulse, the first derivative of Gaussian pulse and the second derivative of the Gaussian pulse [4]. A pulse of width T_p at the subnanosecond scale, occupies UWB with bandwidth $B \approx 1/T_p$ [4]. Such an ultra-short pulse also gives rise to multiple resolvable copies, and thus enables rich multipath diversity [4].

To enable multiple access capability in UWB devices, time-hopping (TH) IR-UWB and direct-sequence (DS) IR-UWB are commonly used. In TH

IR-UWB, each pulse is positioned within each frame duration according to a user-specific TH sequence [4]. Multiple access can also be enabled by modifying the pulse amplitude from frame to frame [4]. In DS UWB impulse radio, each information symbol is direct-sequence modulated using a pseudo-noise (PN) code specific to each user. As these PN codes are orthogonal and known at the transmitter and the receiver, the multiple-access interference is negligible. The TH and DS spreading not only provide multiple access but also smooth the transmit PSD [4].

1.2.2 MC-UWB System

OFDM is a special case of multicarrier transmission that permits subcarriers to overlap in frequency without mutual interference and hence spectral efficiency is increased [6]. The multiband-OFDM UWB is one of the proposed physical layer standard for 802.15.3a WPANs [6]. The idea of multiband technique is to divide the UWB spectrum into subbands with a minimum subband bandwidth of 500 MHz to fulfil the definition assigned by FCC to UWB systems, and use multibanding in conjunction with the OFDM modulation. Thus in multiband-OFDM UWB, each OFDM symbol is transmitted using orthogonal sub-carriers time-interleaved across subbands using time-frequency codes [7]. This approach not only provides frequency diversity but also multiple access [7].

1.3 Motivation of the Work

The transmission of UWB signal over a wireless channel results in multipath components (MPCs) that arrive at the receiver with different attenuation and delay, as also illustrated in Fig. 3.1. As mentioned earlier, due to wide bandwidth, the MPCs arrive with high delay resolution and thus receiver (Rx) is able to resolve many MPCs. The RAKE receiver can be used to receive the MPCs as it exploits the time-diversity inherent in multipth and attempts to collect the signal energy coherently from the received signal paths that fall within its span [14]. However, as the number of resolved MPCs is very high in case of UWB systems, the combining of hundreds of MPCs using RAKE receivers is not realistic. It becomes important to use only a subset of the received MPCs using a specific selection criteria.

The IEEE 802.15.4a group, which has developed a physical layer standard for low data rate systems, has recognized the fact that a considerable amount of UWB devices will be deployed in industrial buildings, factories and warehouses [8]. The application set includes e.g., sensor networks for

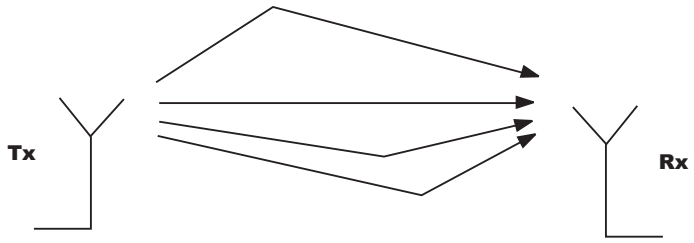

Figure 1.3: An illustration of multipath propagation over a wireless channel, where Tx and Rx stand for the transmitter and receiver, respectively.

process control, supervision of storage halls, asset tagging and management. For such environments like a factory hall with multiple metallic reflectors, the multipath environment is dense and almost all resolvable delay bins contain significant energy [15]. In this case, a RAKE receiver needs to capture a large number of (on the order of hundred) multipath components to collect a significant amount of the received energy [8] [16]. The RAKE receiver design in this case is a challenging task.

Previously, the performance of coherent RAKE and non-coherent receivers for UWB systems has been evaluated in the literature, however, most of these evaluations have been performed using UWB channels for office or residential environments [9], [10], [11], [12], [13]. Moreover, as most of the evaluations are based on simulated channel models employing Rayleigh or Lognormal fading statistics, it is necessary to evaluate the system performance considering realistic channel characteristics of the environment. Thus, the objective of this report is to investigate and analyze the performance of RAKE receivers in terms of uncoded BER for industrial environments using the measured channel responses. The standard channel model proposed by IEEE 802.15.4a for NLOS industrial environments is also used for comparison. The dependence of achievable BER on the types of RAKE, the number of fingers and the RAKE combining schemes is evaluated and compared. Further, based on the simulation results, the conclusions are drawn considering performance and complexity issues of RAKE receiver design for these scenarios.

The rest of the report is organized as follows: the system model of a typical UWB system is described in Chapter 2. Chapter 3 describes the UWB channels used for the performance evaluation of the system and chapter 4 describes RAKE receivers. The simulation parameters and results are discussed in Chapter 5 and finally conclusions are presented in Chapter 6.

Chapter 2

System Model

Considering a binary antipodal modulation and time-hopping impulse radio (TH-IR) UWB system as multiple-access scheme, the transmitted signal from a user in the system can be represented as

$$s(t) = \sqrt{\frac{E_b}{N_f}} \sum_{j=-\infty}^{\infty} d_j b_{\lfloor j/N_{TH} \rfloor} p(t - jT_f - c_j T_c), \tag{2.1}$$

where $p(t)$ is the transmitted UWB pulse, E_b is the symbol energy of the user, T_f is the frame duration, T_c is the chip duration, N_f is the number of pulses representing one binary information symbol $b_{\lfloor j/N_{TH} \rfloor} \in \{1, -1\}$ transmitted by the user. Fig. 2.1 shows an example of the transmitted sequence for a single bit. The pseudorandom time-hopping (TH) sequences $\{c_j\}$ are assigned to each user that share the UWB media to avoid catastrophic collisions among the pulses of different users. If the number of chips in a frame is denoted as N_c, then the chip interval is chosen to satisfy $T_c \leq T_f/N_c$. This avoids pulses of different users from overlapping. The pseudorandom polarity codes $d_j \in \{1, -1\}$ having equal probability provide robustness against multiple access interference [18]. The polarity randomization codes also help to get a zero-mean output and shape the transmit spectrum according to

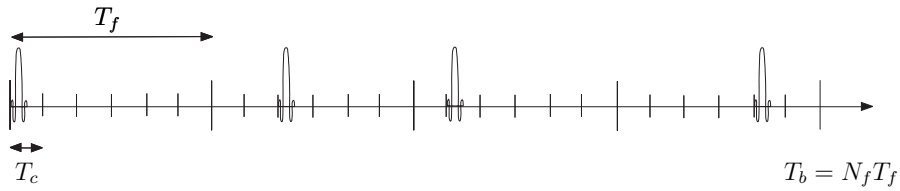

Figure 2.1: An example of the transmitted sequence for a single bit, $N_f = 4$ in this figure.

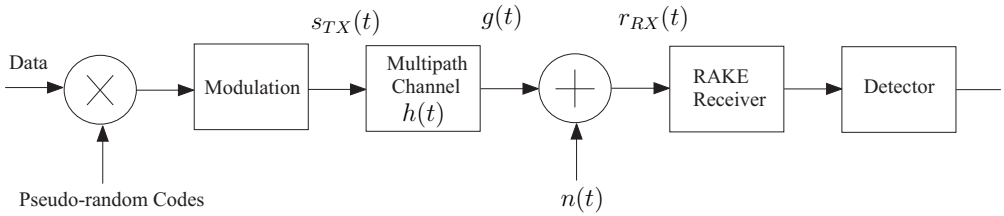

Figure 2.2: Block diagram of the system model (single-user).

FCC rules [17].

The signal for a user is transmitted through a multipath channel with the impulse response given by

$$h(t) = \sum_{k=0}^{K-1} \alpha_k \delta(t - \tau_k), \tag{2.2}$$

where α_k are the channel tap weights, K is the number of multipath components and τ_k is the delay associated with kth multipath component. The details of the channel are described further in the next chapter. The received signal can then be expressed as

$$\begin{aligned} r(t) &= \sqrt{\frac{E_b}{N_f}} \sum_{j=-\infty}^{\infty} \sum_{k=0}^{K-1} \alpha_k d_j b_{\lfloor j/N_{TH} \rfloor} p(t - jT_f - c_j T_c - \tau_k) + n(t) \\ &= \sqrt{\frac{E_b}{N_f}} \sum_{j=-\infty}^{\infty} d_j b_{\lfloor j/N_{TH} \rfloor} g(t - jT_f - c_j T_c) + n(t), \end{aligned} \tag{2.3}$$

where the noise $n(t)$ is a zero mean and $\sigma_n^2 = N_o/2$ variance Gaussian process, and $g(t)$ is interpreted as the aggregate channel after convolving with the transmitted pulse, $g(t) = p(t) * h(t)$, i.e.,

$$g(t) = \sum_{k=0}^{K-1} \alpha_k p(t - \tau_k), \tag{2.4}$$

The duration of $g(t)$ is defined as $T_g = T_p + T_{mds}$, where T_p is the pulse duration, T_{mds} is the maximum delay spread of the channel. The interference between the pulses can be avoided by keeping the delay $T_g \leq T_f$.

Chapter 3

UWB Channel

The received signal in any communications system is an attenuated, delayed, and possibly distorted version of the signal that was transmitted plus noise and (possibly) interference [6]. The relationship between the received signal and the transmitted signal is typically called the "channel" [6]. Previously, most of the work has been performed in the area of narrowband channel modeling and characterization, whereas channel modeling for UWB systems is relatively a new area [5]. The narrowband channel models can not be generalized to UWB channels due to some important differences as described in [5]:

- Each multipath component can lead to delay dispersion by itself, due to frequency-selective nature of reflection and diffraction coefficients. This effect is especially important for systems with large relative bandwidth.
- The signals are received with excellent delay resolution. Therefore, it often happens that only a few multipath components make up one *resolveable* MPC. That implies that the cental limit theorem is not fulfilled anymore, and the amplitude statistics of such a resolvable MPC is not complex Gaussian anymore. Similarly, there is an appreciable probability that areas of "no energy" can exist during which no significant amount of energy is arriving at the receiver.
- The statistics of arrival times of multipath components strongly vary with the bandwidth, as well as with the center frequency of the considered signal.
- Due to wide frequency band, the propagation signals experience frequency dependent effects. Specifically, the path loss is described as a function of frequency as well as of distance when the relative bandwidth is large.

In the following sections, the IEEE 802.15.4a channel model and the measured channels in an industrial environment are discussed.

3.1 UWB Channel Model (IEEE 802.15.4a)

The IEEE 802.15.4a group has proposed a channel model for sensor networks and similar devices with data rates between 1 kbit/s and several Mbit/s. The important features of the channel model are discussed in the next sections.

3.1.1 Path loss and shadowing

The large-scale channel modeling involves modeling the signal attenuation with distance and is generally referred to as path loss [6]. The path loss in a narrowband system is conventionally defined as [19],

$$PL(d) = \frac{E\{P_{RX}(d, f_c)\}}{P_{TX}} \tag{3.1}$$

where P_{TX} and P_{RX} are the transmit and receive power, respectively, d is the distance between transmitter and receiver, f_c is the center frequency and the expectation $E\{\}$ is taken over an area that is large enough to allow averaging out of shadowing as well as the small-scale fading. Due to the frequency dependence of propagation effects in a UWB channel, the wideband path loss is a function of frequency as well as of distance [19]. It thus makes sense to define a *frequency-dependent path loss* as [19],

$$PL(d, f) = E\{\int_{f-\Delta f/2}^{f+\Delta f/2} |H(\tilde{f}, d)|^2 d\tilde{f}\} \tag{3.2}$$

where $H(\tilde{f}, d)$ is the transfer function from transmitting antenna connector to the receiving antenna connector, and Δf is chosen small enough so that diffraction coefficients, dielectric constants, etc., can be considered constant within that bandwidth. The total path loss is obtained by integrating over the whole bandwidth of interest [19].

It is assumed that the path loss as a function of frequency and distance can be written as a product of the terms [19],

$$PL(d, f) = PL(f)PL(d) \tag{3.3}$$

The frequency dependence of the path loss is given as [20],[21],

$$\sqrt{PL(f)} \propto f^{-\kappa} \tag{3.4}$$

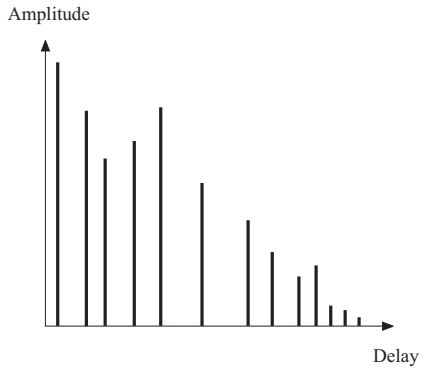

Figure 3.1: Multipath components with different attenuations and delays.

where κ is the frequency dependence factor. The distance dependence of the path loss in dB is described by [19],

$$PL(d) = PL_o + 10n \log_{10}\left(\frac{d}{d_o}\right) \tag{3.5}$$

where the reference distance d_o is set to 1 m, PL_o is the path loss at the reference distance, and n is the path loss exponent. The path loss exponent depends on the environment and on whether a line-of-sight (LOS) connection exists between the transmitter and receiver or not [19].

The variation in the received signal power about its mean value is typically termed "shadowing" [6]. The path loss (averaged over small-scale fading) in dB can be written as [19],

$$PL(d) = PL_o + 10n \log_{10}\left(\frac{d}{d_o}\right) + S \tag{3.6}$$

where S accounts for shadowing and is a Gaussian distributed random variable with zero mean and the standard deviation σ_s.

3.1.2 Power delay profile

Power delay profile (PDP) relates the power of the received signal with the delay experienced by the multipath component and is defined as the square magnitudes of the impulse response of the signal averaged over a local area as [22],

$$PDP(\tau) = |h(t;\tau)|^2 \tag{3.7}$$

The impulse response (in complex baseband) is based on the SV (Saleh-Valenzuela) model which is given in general as [23],

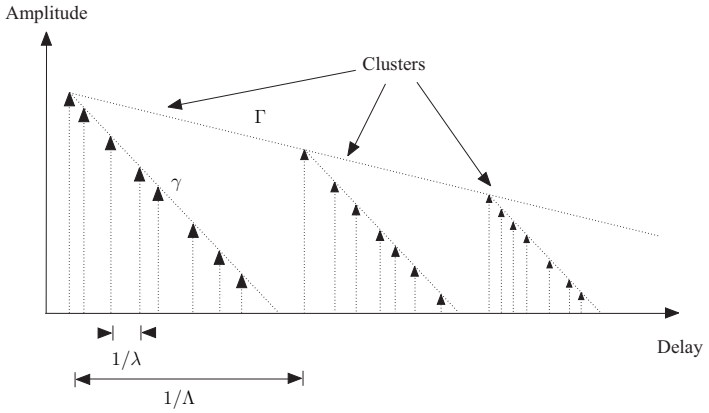

Figure 3.2: Principle of Saleh-Valenzuela model.

$$h_{discr}(t) = \sum_{l=0}^{L-1} \sum_{k=0}^{K-1} \alpha_{k,l} \exp(j\phi_{k,l}) \delta(t - T_l - \tau_{k,l}), \tag{3.8}$$

where $\alpha_{k,l}$ is the tap weight of the kth component (path) in the lth cluster, T_l is the arrival time of the lth cluster and $\tau_{k,l}$ is the delay of the kth MPC relative to the the lth cluster arrival time T_l, see Fig. 3.2. The phases $\phi_{k,l}$ are uniformly distributed, i.e. for a bandpass system, the phase is taken as a uniformly random variable in the range from $[0, 2\pi]$ [19].

The number of clusters L is an important parameter of the model and is assumed to be Poisson-distributed [19],

$$pdf_L(L) = \frac{(\bar{L})^L \exp(-\bar{L})}{L!} \tag{3.9}$$

so that the mean $\bar{L}$ completely characterizes the distribution.

The distribution of cluster arrival times are given by a Poisson process [19],

$$p(T_L|T_{L-1}) = \Lambda_l \exp[-\Lambda_l(T_L - T_{L-1})], l > 0 \tag{3.10}$$

where Λ_l is the cluster arrival rate.

The ray arrival times are modeled with mixtures of two Poisson processes as follows [19],

$$\begin{aligned} p(\tau_{k,l}|\tau_{(k-1),l}) &= \beta\lambda_1 \exp[-\lambda_1(\tau_{k,l} - \tau_{(k-1),l})] \\ &+ (\beta - 1)\lambda_2 \exp[-\lambda_2(\tau_{k,l} - \tau_{(k-1),l})], k > 0 \end{aligned} \tag{3.11}$$

where β is the mixture probability, while λ_1 and λ_2 are the ray arrival rates.

The power delay profile (the mean power of different paths) is exponential within each cluster [19],

$$E\{|a_{k,l}|^2\} = \Omega_l \frac{1}{\gamma_l[(1-\beta)\lambda_1 + \beta\lambda_2 + 1]} \exp(-\tau_{k,l}/\gamma_l) \tag{3.12}$$

where Ω_l is the integrated energy of the lth cluster and γ_l is the intra-cluster decay time constant.

Further, the mean (over cluster-shadowing) mean (over small-scale fading) energy (normalized to γ_l) of the lth cluster follows in general exponential decay [19],

$$10\log(\Omega_l) = 10\log(\exp(-T_l/\Gamma)) + M_{cluster} \tag{3.13}$$

where $M_{cluster}$ is normally distributed random variable with standard deviation $\sigma_{cluster}$ around it.

Finally, the cluster decay rates are found to depend linearly on the arrival time of the cluster [19],

$$\gamma_l = k_\gamma T_l + \gamma_o \tag{3.14}$$

where k_γ describes the increase of the decay constant with delay.

In this model, particularly for some NLOS scenarios (office and industrial), the shape of the power delay profile (PDP) can be different, namely (on a log-linear scale) [19],

$$\begin{aligned} E\{|a_{k,l}^2|\} = {} & (1 - \chi \exp(-\tau_{k,l}/\gamma_{\text{rise}})) \exp(-\tau_{k,l}/\gamma_1) \\ & \cdot \frac{\gamma_1 + \gamma_{\text{rise}}}{\gamma_1} \frac{\Omega_1}{\gamma_1 + \gamma_{\text{rise}}(1-\chi)}, \end{aligned} \tag{3.15}$$

where the parameter χ describes the attenuation of the first component, the parameter γ_{rise} determines how fast the PDP increases to its local maximum, and γ_1 determines the decay at late times.

3.1.3 Delay dispersion

Delay dispersion is defined to occur when the channel impulse response lasts for a finite amount of time or channel is frequency selective [5]. Delay dispersion in multipath channels is characterized by two important parameters, mean excess delay and root mean square (rms) delay spread [5].

Excess delay is the relative delay of kth received multipath component as compared to the first arriving path, and is denoted as τ_k [22]. *Mean excess delay* is defined as the first moment of the PDP given by [22],

$$\tau_m = \frac{\int_{-\infty}^{\infty} PDP(\tau)\tau d\tau}{\int_{-\infty}^{\infty} PDP(\tau)d\tau} \tag{3.16}$$

The rms delay spread is defined as the second central moment of the PDP given by [19],

$$\tau_{rms} = \sqrt{\frac{\int_{-\infty}^{\infty} PDP(\tau)\tau^2 d\tau}{\int_{-\infty}^{\infty} PDP(\tau)d\tau} - \left(\frac{\int_{-\infty}^{\infty} PDP(\tau)\tau d\tau}{\int_{-\infty}^{\infty} PDP(\tau)d\tau}\right)^2} \tag{3.17}$$

The delay spread depends on the distance, however, this effect is neglected in the channel model for simplicity [19].

3.1.4 Small scale fading

The rapid fluctuations of the received signal strength over very short travel distances (of few wavelengths) or short time durations (on the order of seconds) is called small-scale fading [22]. In this model, the distribution of small scale amplitudes is Nakagami [19],

$$pdf(x) = \frac{2}{\Gamma(m)}(\frac{m}{\Omega})^m x^{2m-1} \exp(-\frac{m}{\Omega}x^2), \tag{3.18}$$

where $m \geq 1/2$ is the Nakagami $m-$factor, $\Gamma(m)$ is the gamma function, and Ω is the mean-square value of the amplitude i.e., mean power. The $m-$parameter is modeled as a lognormally distributed random variable, logarithm of which has a mean μ_m and a standard deviation σ_m [19]. Both of these values can have a delay dependence [19],

$$\mu_m(\tau) = m_o - k_m\tau \tag{3.19}$$

$$\sigma_m = \widehat{m}_o - \widehat{k}_m\tau \tag{3.20}$$

For the first component of each cluster, the Nakagami factor is assumed to be deterministic and independent of delay [19],

$$m = \tilde{m}_o. \tag{3.21}$$

The IEEE 802.15.4a channel model covers different office, residential and industrial scenarios. The channel model which is used for performance evaluation of RAKE receiver is for NLOS scenarios in industrial environments, referred to as CM8.

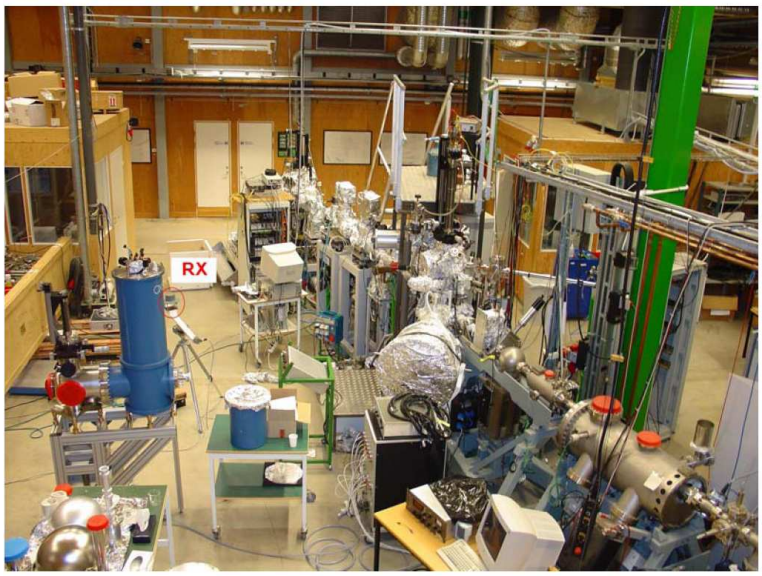

Figure 3.3: An overview of the environment of the measured UWB channels.

3.2 Measured UWB Channels

The UWB channel measurement campaign had been conducted together with Lund university in MAX-Lab, Lund, Sweden, a medium-sized industrial environment. The hall has a floor area of 94×70 m and a ceiling height of 10 m. The hall contains many metallic objects, pipes, pumps and cylinders. The measurements were performed in the frequency domain using a vector network analyzer (VNA) in conjunction with virtual antenna arrays. The frequency range measured was from 3.1 to 8.0 GHz. 2001 frequency points were measured, resulting in a delay resolution of 0.2 ns, and a maximum delay of 408 ns corresponding to 122 m path delay. Omnidirectional conical monopole antenna were used at transmitter and receiver, respectively. The use of virtual antenna arrays allows to create a virtual MIMO system of 7×7 antenna positions. The antenna separation was 50 mm, i.e., more than half a wavelength at the minimum frequency in order to obtain spatially independent channels. Thus, for each measurement, 49 independent realizations of the channel were measured over a local area resulting in a total of 49×16 independent NLOS channel realizations. A total of sixteen peer-to-peer (P-P) NLOS positions were measured at four different locations with Tx-Rx separations of 2 m, 4 m, 8 m and 16 m at each location. A complete description of the measurement setup and analysis of the model parameters can be found in [8].

3.2.1 Measured Power Delay Profiles

The measured transfer functions were transformed to the delay domain using inverse Fourier transformation with a hanning window applied. The power delay profiles (PDPs) calculated from the measurements on one antenna pair of the virtual array are called instantaneous PDPs, where the PDP from the n-th transmitter to the m-th receiver is defined as [8],

$$PDP(\tau, m, n) = |h(\tau, m, n)|^2. \tag{3.22}$$

Average power delay profiles (APDPs) were obtained from 49 instantaneous PDPs corresponding to the different combinations of transmitter and receiver positions on the virtual array for each of the measurement positions. Thus, APDPs were obtained as [8],

$$APDP(\tau) = \frac{1}{MN} \sum_{m=1}^{M} \sum_{n=1}^{N} PDP(\tau, m, n). \tag{3.23}$$

The analysis of APDPs for P-P NLOS measurements has shown the following effects [8]:

1. For shorter distances (and a few of longer distance measurements), the first component is the strongest. A similar observation was also made in [15] for industrial environments.

2. The strong first component is followed by a minimum in the APDP indicating that the multipath components arrive in clusters.

3. For many of the measurements at larger distances, the strongest component arrives $10 - 40$ ns after the first arriving component.

4. For longer distances, the APDP has "soft-onset" shape as also seen in [15].

5. It has been observed that some specific MPCs carry significant power for larger Tx-Rx separations.

6. It is also observed that nearly all resolvable delay bins contain significant energy

3.2.2 Comparison of channel characteristics

The measured channel responses are divided into two groups based on the Tx-Rx separation. The *measurement group* 1 (MG1) covers the distances in

Table 3.1: Comparison of Channel Characteristics

Channel characteristics	**MG1**	**MG2**	**CM8**
Distance (m)	2–8	10–16	2–8
Scenario	NLOS	NLOS	NLOS
Mean excess delay [ns]	43	62.9	113.3
RMS delay spread [ns]	51	66	87
$NP_{10[dB]}$	47.1	86.5	220.9
NP{85%}	209.8	318.1	1137.2

the range of 2 to 8 m, while the *measurement group* 2 (MG2) consists of the measured channel responses with Tx-Rx separation from 10 to 16 m. The total number of independent realizations for MG1 and MG2 are 490 and 294, respectively.

For the performance comparison with the measured channels, 100 realizations of CM8 are simulated using the channel model parameters. A comparison of some characteristics averaged over different realizations of the channels is given in Table II. $NP_{10[dB]}$ is the average number of paths within 10 [dB] of the strongest path in the channel and NP {85%} denotes the average number of paths that contain 85 percent of the channel energy. Moreover, average power delay profiles (APDPs) of MG1, MG2 and CM8 averaged over all channel realizations are shown in Fig. 3.4.

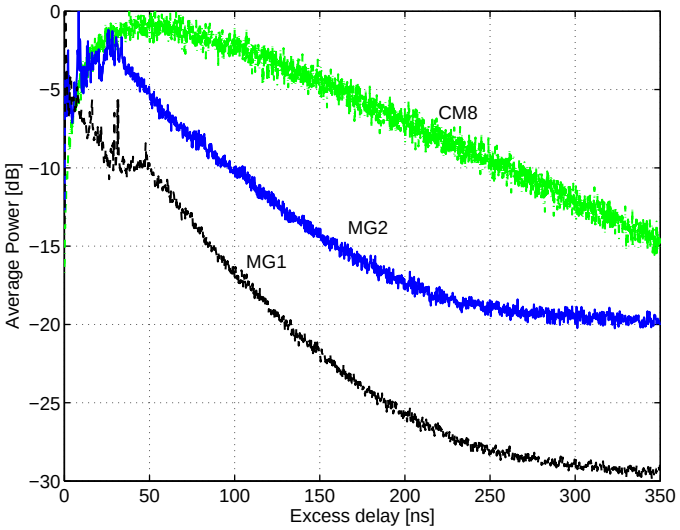

Figure 3.4: Average power delay profiles of MG1, MG2 and CM8 averaged over all channel realizations.

Chapter 4

RAKE Receivers

4.1 Introduction

The amount of multipath energy that can be collected at the receiver and the receiver complexity are commonly used to determine the performance and robustness of a wireless communication system [7]. The RAKE receiver is used in any kind of spread spectrum communication system to accumulate the energy in the significant multipath components [6]. The use of RAKE receiver in UWB systems is also common to collect the available rich multipath diversity.

A RAKE receiver consists of a bank of correlators, also called fingers, and each finger is matched (synchronized) to a particular multipath component to combine the received multipaths coherently [6]. In order to enable *symbol-rate* sampling, the received IR-UWB signal can be correlated with a symbol-length template signal, and the correlator output can be sampled once per symbol [26]. The drawback of RAKE receiver is that the number of multipath components that can be utilized in a typical RAKE combiner is limited by power consumption issues, design complexity, and the channel estimation [24]. Secondly, each multipath undergoes a different channel in UWB systems, which causes distortion in the received pulse shape and makes the use of a single LOS path signal as a suboptimal template [25].

4.2 RAKE Types

A tapped delay line channel with K number of delays provides us with K replicas of the same transmitted signal at the receiver [6]. Hence, a receiver that processes the received signal in an optimum manner will achieve the performance of an equivalent Kth order diversity system [6]. In practice, only a

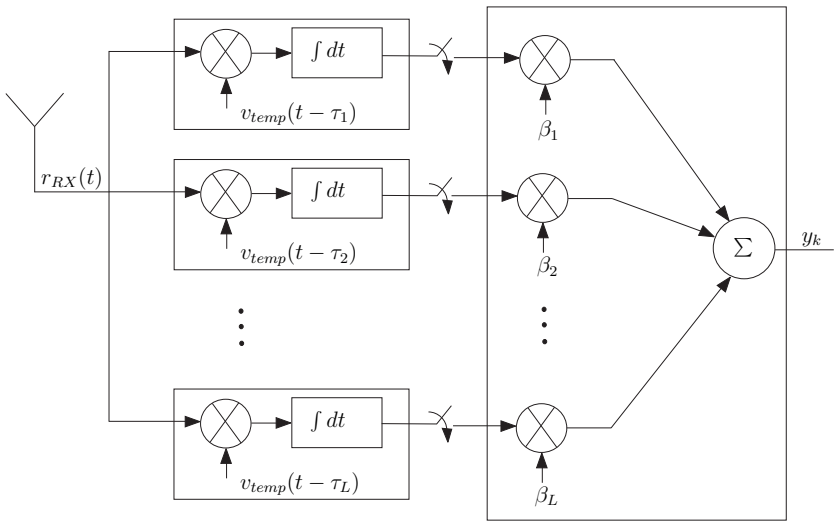

Figure 4.1: A RAKE receiver structure for TH-IR UWB system.

subset of total resolved multipath components is used in the RAKE receivers [24]. The RAKE types based on the number of multipath components used are given as follows [24],

- All RAKE (*ARake*): The RAKE receiver which combines all the K resolved multipath components is called all RAKE (*ARake*).
- Selective RAKE (*SRake*): The SRake receiver searches for the M *best paths* out of K resolved MPCs to use them as RAKE fingers.
- Partial RAKE (*PRake*): The PRake receiver uses the M *first arriving* paths out of K resolvable multipath components.

4.3 RAKE Combining Schemes

The outputs of the correlators (fingers) are passed to the RAKE combiner. The RAKE receiver can use different combining schemes such as maximal ratio combining (MRC) and equal gain combining (EGC) scheme.

4.3.1 Maximal Ratio Combining (MRC)

If maximal ratio combining (MRC) technique is used, the amplitudes of the received MPCs are estimated and used as weighing vector in each finger.

The performance and optimality of the MRC consequently depend upon the receiver's knowledge of the channel [25]. Let $\boldsymbol{\beta} = [\beta_0, \beta_1, \cdots, \beta_{K-1}]$ be the RAKE combining weights which are different for different RAKE types.

- In case of ARake, the combining weights are chosen equal to the fading coefficients of the channel, $\boldsymbol{\alpha} = [\alpha_0, \alpha_1, \cdots, \alpha_{K-1}]$, i.e.,

$$\boldsymbol{\beta} = \boldsymbol{\alpha} \tag{4.1}$$

- For SRake, if the set of indices of the M best fading coefficients with largest amplitude is denoted by $\mathcal{S}$, then the combining weights $\boldsymbol{\beta}$ are chosen as follows [27],

$$\boldsymbol{\beta} = \begin{cases} \alpha_k, & k \in \mathcal{S} \\ 0, & k \notin \mathcal{S} \end{cases} \tag{4.2}$$

- For PRake, using the first M multipath components, the weights of MRC combining are given by [27],

$$\boldsymbol{\beta} = \begin{cases} \alpha_k, & k = 0, \cdots, M-1 \\ 0, & k = M, \cdots, K-1 \end{cases} \tag{4.3}$$

  where $M \leq K$.

4.3.2 Equal Gain Combining (EGC)

In case of equal gain combining (EGC) scheme, all the tracked MPCs are weighted with their corresponding signs and combined [9]. Thus, EGC combining scheme only requires the phase of the fading channel [28]. In a carrierless UWB system, determining the phase is even simpler because the phase is either 0 or π, to account for pulse inversion [29]. In a practical system, performing EGC will be simpler than MRC but there will be a performance trade-off [28].

4.4 Analysis of RAKE Receiver

In this section, it is assumed that we have perfect knowledge of the channel and *ARake* receiver is used to receive the IR-UWB signal discussed in Chapter 2. Considering the ith symbol, the output of the kth finger of the receiver can be written as

$$y_{i,k} = \int_{-\infty}^{+\infty} r_i(t) v_{temp}(t - \tau_k) dt, \qquad (4.4)$$
$$k = 0, 1, \cdots, K-1 \text{ for each } i$$

where $v_{temp}(t)$ is assumed to be the normalized template signal matched to the whole pulse sequence of one information symbol, i.e.,

$$v_{temp}(t) = \sqrt{\frac{1}{N_f}} \sum_{j=0}^{N_f - 1} d_j p(t - jT_f - c_j T_c), \qquad (4.5)$$
$$0 \le t \le N_f T_f$$

and $r_i(t)$ is the received signal for ith bit, which is given by

$$r_i(t) = \sqrt{\frac{E_b}{N_f}} \sum_{j=0}^{N_f - 1} d_j b_i g(t - jT_f - c_j T_c) + n(t). \qquad (4.6)$$

The analysis of RAKE receiver is further discussed based on the assumptions of resolvable and nonresolvable paths.

4.4.1 Resolvable Paths

It is assumed that all paths are resolvable, that is, the minimum time between any two paths is larger than the pulse width [6]. Let us define the cross-correlation function between $g(t)$ and $p(t)$ as [25],

$$\alpha(\tau) = \int_{-\infty}^{\infty} g(t) p(t - \tau), \qquad (4.7)$$

where $\alpha(\tau) = 0$ if $\tau \le -T_p$ or $\tau \ge T_g$. If there is a perfect match of the received signal with the reference signal, zero inter-frame and inter-symbol interference, then the output of kth finger after summation over N_f frames of ith symbol can be written in discrete time as

$$y_{i,k} = \sqrt{E_b} b_i \alpha_k + \eta_{i,k}, \qquad (4.8)$$
$$k = 0, 1, \cdots, K-1 \text{ for each } i$$

where the last term $\eta_{i,k} = \int_{-\infty}^{+\infty} n(t) v_{temp}(t - \tau_k) dt$ is the noise at the output of the correlator which has zero mean and variance σ_n^2.

All fingers of the RAKE use a delayed version of the template signal $v_{temp}(t)$, with a delay chosen from the vector $\boldsymbol{\tau} = [\tau_0 . \cdots, \tau_{K-1}]^T$, to match it

to a specific multipath component. The outputs of all the fingers (correlators) for the ith symbol can be written together in vector notation as

$$\mathbf{y}_i = \sqrt{E_b} b_i \boldsymbol{\alpha} + \boldsymbol{\eta}_i, \tag{4.9}$$

where $\mathbf{y}_i = [y_{i,0}, \cdots, y_{i,K-1}]^T$, $\boldsymbol{\alpha} = [\alpha_0. \cdots, \alpha_{K-1}]^T$, and $\boldsymbol{\eta}_i = [\eta_{i,0}, \cdots, \eta_{i,K-1}]^T$.

Further, the diversity combining using the weight vector $\boldsymbol{\beta}$ yields the decision statistic for ith bit as

$$z_i = \boldsymbol{\beta}^T \mathbf{y}(i) \tag{4.10}$$

$$= \sqrt{E_b} b_i \sum_{k=0}^{K-1} \beta_k \alpha_k + \sum_{k=0}^{K-1} \beta_k \eta_{i,k}, \tag{4.11}$$

for ARake receiver with MRC combining, $\boldsymbol{\beta} = \boldsymbol{\alpha}$, thus

$$z_i = \sqrt{E_b} b_i \sum_{k=0}^{K-1} \beta_k^2 + \sum_{k=0}^{K-1} \beta_k \eta_{i,k}. \tag{4.12}$$

To determine the bit error probability (BEP) at the output of the RAKE, the approximate mean and variance of the decision statistic at the output of RAKE from (4.20) are evaluated as

$$E[z_i] = \sqrt{E_b} \sum_{l=0}^{K-1} \beta_k^2, \tag{4.13}$$

$$\mathrm{Var}(z_i) = \sigma_n^2 \sum_{k=0}^{K-1} \beta_k^2. \tag{4.14}$$

In case of binary antipodal modulation, the approximate expression of BEP conditioned on a particular channel realization is given by [25],[14],

$$\begin{aligned} P_{e|(\boldsymbol{\alpha},\boldsymbol{\tau})} &= Q\left(\sqrt{\frac{E[z_i|(\boldsymbol{\alpha},\boldsymbol{\tau})]^2}{\mathrm{Var}(z_i|(\boldsymbol{\alpha},\boldsymbol{\tau}))}}\right) \\ &= Q\left(\sqrt{\frac{E_b\Big(\sum_{k=0}^{K-1} \beta_k^2\Big)^2}{\sigma_n^2 \sum_{k=0}^{K-1} \beta_k^2}}\right) \\ &= Q\left(\sqrt{\frac{2E_b}{N_o} \sum_{k=0}^{K-1} \beta_k^2}\right), \end{aligned} \tag{4.15}$$

here $Q(\cdot)$ is the standard function $Q(x) = 1/\sqrt{2\pi} \int_x^\infty e^{-t^2/2} dt$ [25].

4.4.2 Nonresolvable Paths

Assuming that the two paths may be less than a pulse width apart, the autocorrelation function of the wave is now evident [6]. The output of kth finger for ith symbol can be written as

$$y_{i,k} = \sqrt{E_b} b_i \alpha_k + \sqrt{E_b} b_i \sum_{j=0, j\neq k}^{K-1} \alpha_j R(\tau_j - \tau_k) + \tilde{\eta}_{i,k} dt, \qquad (4.16)$$
$$k = 0, 1, \cdots, K-1 \text{ for each } i$$

where $R(\tau)$ is the autocorrelation of the pulse $p(t)$, defined as

$$R(\tau) = \int_{-\infty}^{\infty} p(t) p(t-\tau) dt, \qquad (4.17)$$

and $\tilde{\eta}_{i,k}$ is the noise with zero mean and variance $\sigma_n^2 \sum_{j=0}^{K-1} \alpha_j R(\tau_j - \tau_k)$ [6].

The outputs of all the fingers can be written in vector form as $\mathbf{y}_i = [y_{i,0}, \cdots, y_{i,K-1}]^T$, then the decision statistic is formed using the diversity combining, i.e.,

$$z_i = \boldsymbol{\beta}^T \mathbf{y}(i) \qquad (4.18)$$
$$= \sqrt{E_b} b_i \sum_{k=0}^{K-1} \beta_k \alpha_k + \sqrt{E_b} b_i \sum_{k=0}^{K-1} \sum_{j=0, j\neq k}^{K-1} \beta_k \alpha_j R(\tau_j - \tau_k) + \sum_{k=0}^{K-1} \beta_k \tilde{\eta}_{i,k}, \qquad (4.19)$$

as for ARake receiver with MRC combining, $\boldsymbol{\beta} = \boldsymbol{\alpha}$, thus

$$z_i = \sqrt{E_b} b_i \left[\sum_{k=0}^{K-1} \beta_k^2 + \sum_{k=0}^{K-1} \sum_{j=0, j\neq k}^{K-1} \beta_k \beta_j R(\tau_j - \tau_k) \right] + \sum_{k=0}^{K-1} \beta_k \tilde{\eta}_{i,k}. \qquad (4.20)$$

The approximate mean and variance of the decision statistic at the output of RAKE are evaluated as [6],

$$E[z_i] = \sqrt{E_b} \left[\sum_{k=0}^{K-1} \beta_k^2 + \sum_{k=0}^{K-1} \sum_{j=0, j\neq k}^{K-1} \beta_k \beta_j R(\tau_j - \tau_k) \right], \qquad (4.21)$$

$$\mathrm{Var}(z_i) = \sigma_n^2 \sum_{k=0}^{K-1} \sum_{j=0}^{K-1} \beta_k \beta_j R(\tau_j - \tau_k). \qquad (4.22)$$

The approximate expression of BEP conditioned on a particular channel realization is given by [6],

$$P_{e|(\boldsymbol{\alpha},\boldsymbol{\tau})} = Q\left(\sqrt{\frac{2E_b}{N_o}\frac{\left[\sum_{k=0}^{K-1}\beta_k^2 + \sum_{k=0}^{K-1}\sum_{j=0,j\neq k}^{K-1}\beta_k\beta_j R(\tau_j-\tau_k)\right]^2}{\sum_{k=0}^{K-1}\sum_{j=0}^{K-1}\beta_k\beta_j R(\tau_j-\tau_k)}}\right), \tag{4.23}$$

where $\sum_{k=0}^{K-1}\sum_{j=0,j\neq k}^{K-1}\beta_k\beta_j R(\tau_j-\tau_k)$ represents the additional term due to path correlations. Because the delays and amplitudes of of the RAKE fingers will be shifted when path correlations are nonzero, the development of (4.23) is a simplified analysis [6].

Chapter 5

Simulation Results

In order to compare the performance of RAKE receivers on the NLOS multipath channels described in chapter 4, the UWB system is simulated for an indoor industrial environment. The simulation parameters are as follows:

- The binary antipodal modulation is used employing second derivative of the Gaussian pulse.
- The pulse duration is kept 1.02 ns and 0.625 ns over measured and simulated channels, respectively.
- The uncoded data rate of 4 Mbps is achieved with $N_f = 10$ and $T_f = 25$ ns.
- A frame time of $T_f = 25$ ns results in inter-frame interference (IFI) as it is less than the delay spread introduced by the channels.
- The energy of the channel impulse response is normalized as $\sum \alpha_l^2 = 1$.
- The system is assumed to be synchronized with perfect knowledge of the channel characteristics.
- For each E_b/N_o, the performance over channel models is evaluated using 490, 294 and 100 channel realizations of MG1, MG2 and CM8, respectively.
- The simulations are performed until 200 bit errors has been detected or at least $100,000$ bits has been transmitted.
- It should be emphasized that these are uncoded bit-error-rates which can be improved by using different coding techniques.

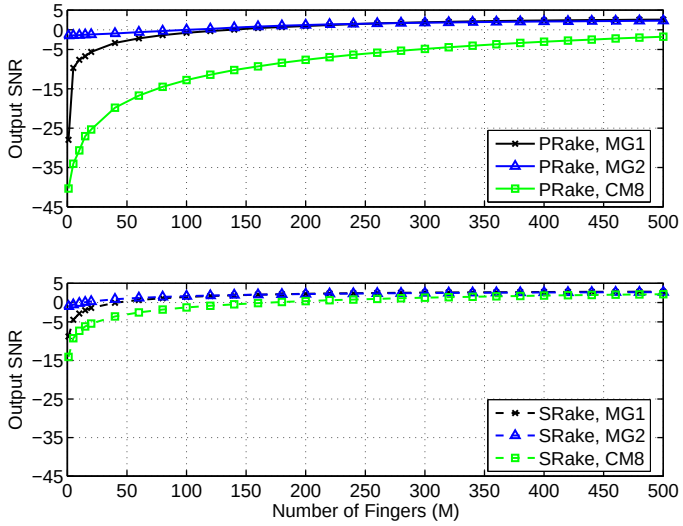

Figure 5.1: Output SNR vs Number of RAKE fingers on MG1, MG2 and CM8 PRake (top) and SRake(bottom).

In Fig. 5.1, the analytical expression of (4.21) and (4.22) are averaged for each channel over corresponding number of realizations. The output SNR (SNR_o) is shown versus the number of MPCs captured by PRake and SRake over MG1, MG2 and CM8. The results demonstrate an increase in SNR_o with the increase in number of fingers. It is observed that the increase in SNR with the increase in number of captured MPCs is low for PRake as compared to SRake. Moreover, the dependence of SNR_o over the channel models is also observed. The gain in SNR_o as the number of fingers increases is much higher in case of MG1 up to a certain number of fingers. It is noteworthy that this is particularly depicted by PRake receiver. It is also observed that the SNR improvement is significant by increasing the number of fingers up to 100 for PRake and 50 for SRake. However, the saturation effects are observed by any further increase as the rest of the components do not carry significant energy. It can be concluded that any further increase in the number of fingers increases the complexity of the system and does not provide much SNR gain. This is particularly true for the channels having a shape of the PDP similar to MG1 and MG2.

Fig. 5.2 presents the results of PRake receiver with MRC combining using different number of fingers. The results are shown for both measured and simulated channels. The results demonstrate that the performance of PRake receiver largely depends on the shape of channel profile. As PRake captures

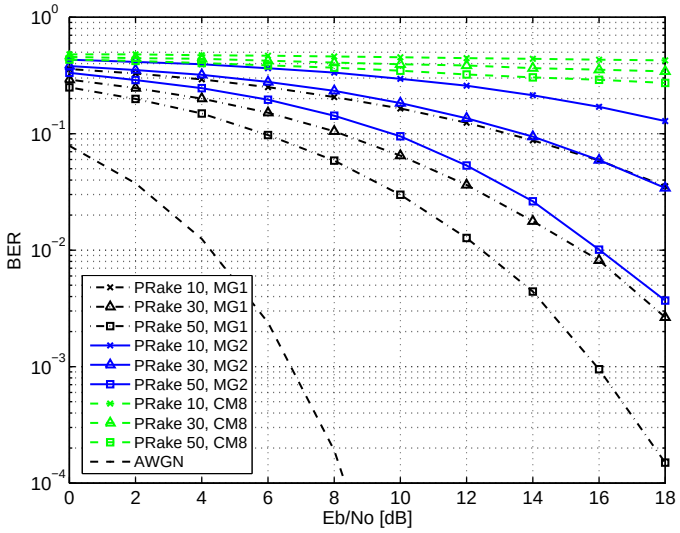

Figure 5.2: Comparison of BER of different number of fingers of PRake with MRC combining on MG1, MG2 and CM8.

only the first arriving components, the performance severely degrades on CM8 as compared to MG1 and MG2. This is quite intuitive as CM8 has first increasing and then decreasing power delay profile. The power delay profile of MG2 also has a shape of first increasing and then decreasing PDP, see Fig. 3.4. However, in contrast to CM8, the PDP of MG2 has a fast increase to its local maximum and also the decay is fast at late times. In addition, there are some strong components in the PDP indicating the arrival of MPCs in clusters. On the other hand, MG1 has a decreasing PDP with embedded strong components at shorter delays indicating the onset of clusters of MPCs.

It is shown in Fig. 5.2 that the BER is very high even with 50 PRake fingers particularly over CM8. To further improve the BER, PRake need to use on the order of hundred fingers that increases the complexity of the receiver significantly. In the case of MG2, a BER of 10^{-2} is achieved using $M = 50$ fingers with $E_b/N_o = 16$ dB. However, the results show that by using 30 fingers of the PRake receiver, it is not possible to achieve a BER of 10^{-2} even with a further increase in E_b/N_o of 2 dB.

In Fig. 5.3, the performance of SRake receiver has been analyzed using different number of fingers with MRC combining. The results demonstrate a significant performance improvement using SRake as compared to PRake. The results for CM8 indicate that it is possible to achieve a BER of 10^{-2} with $E_b/N_o = 16$ dB using 30 fingers of the SRake.

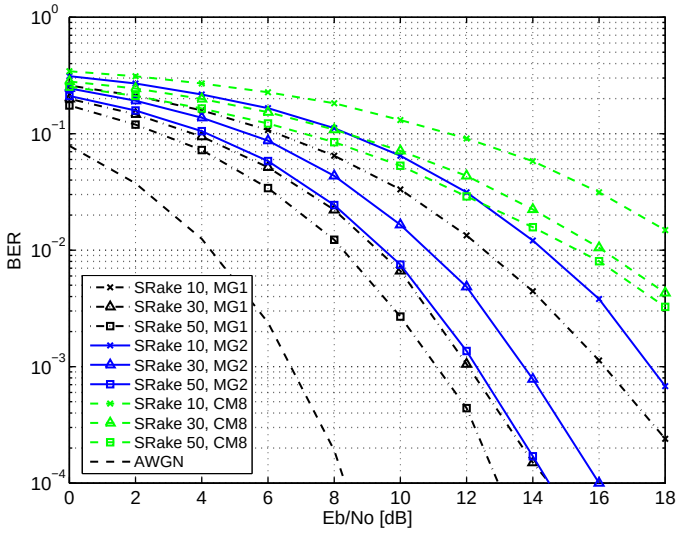

Figure 5.3: Comparison of BER of different number of fingers of SRake with MRC combining on MG1, MG2 and CM8.

The results over channel MG2 show that 30 SRake fingers can provide a BER of 10^{-3} with $E_b/N_o = 13.5$ dB . It is also observed that the same BER can be achieved using only 10 fingers of SRake over MG2 with $E_b/N_o = 16.5$ dB. Moreover, the performance of SRake is also better over channel MG1, as compared to the performance over MG2 and CM8. For MG1, the results of Fig. 5.3 demonstrate that a BER of 10^{-3} is achieved with only 10 fingers of the SRake with $E_b/N_o = 16$ dB. Moreover, the same BER of about 10^{-3} is achieved with $E_b/N_o = 12$ dB when 30 fingers of the SRake receiver are used.

When compared with PRake receiver, it is observed that SRake can achieve much better performance. This is particularly true for the channels having a shape of the PDP similar to CM8. In case of MG2, the SRake performance using only 10 fingers is better than using 50 fingers of PRake. While for MG1, the results demonstrate that 10 fingers of SRake has almost the same BER as the 50 fingers of the PRake. These results depict a significant performance improvement associated with the SRake that uses only few fingers. However, it should be mentioned that the complexity of the SRake stems from the fact that it needs to search for the 10 fingers that carry the maximum energy.

The effect of RAKE combining scheme is analyzed in Fig. 5.4. The BER is compared using 30 fingers of both types of RAKE using EGC and MRC

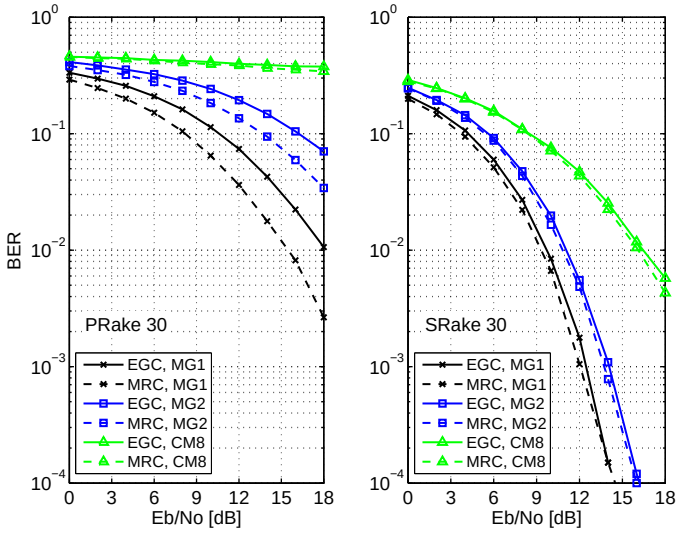

Figure 5.4: Comparison of EGC and MRC combining using 30 fingers of PRake (left) and SRake (right) on MG1, MG2 and CM8.

combining schemes. The results show that the performance of MRC combining is better than EGC. It should be noted that, over measured channels with PRake, there is some performance improvement using MRC rather than EGC combining. In contrast, the BER using EGC and MRC is almost comparable in case of SRak. In this case, the complexity of the SRake can be reduced using EGC without a significant performance degradation.

Chapter 6

Conclusions

The performance evaluation of different types of RAKE receivers using measured and simulated NLOS channels for industrial environments is presented. The analysis of the results shows that, for measured channels with shorter Tx-Rx separation (i.e. 2–8 m), a moderate number of fingers of SRake (i.e. about 10 fingers) are required to achieve an acceptable BER. For larger Tx-Rx separation (i.e. 10–16 m), SRake requires 1.5 dB more E_b/N_o to achieve the same BER performance. On the other hand, PRake receiver is unable to achieve the same BER performance even with a large number fingers. For simulated IEEE 802.15.4a channel, the PRake receiver has very poor performance, while the SRake receiver provides significant improvement in the performance.

The above results demonstrate that the SRake receiver always outperforms the PRake using the same number of fingers and the same combining scheme. It is observed that the performance of the RAKE receivers degrades as the Tx-Rx distance increases. It can also be concluded that the difference in the performance of MRC and EGC combining schemes is not that significant for SRake, while PRake has a considerably better performance using MRC. The PRake receiver with MRC combining can be used if the first arriving multipath components carry significant energy which is common in case of shorter Tx-Rx separations. The SRake receiver with either EGC or MRC combining should be used if the first arriving components are not the strongest, which is typical for larger Tx-Rx separations. Further, the comparison of results demonstrates that the performance of receiver is better over measured channels as compared to the simulated channels. Hence, the performance of receiver depends to a large extent on the underlying channel and the shape of the power delay profile. It can be concluded that the simulated channels for industrial environments can not be generalized for all such environments as the propagation characteristics can differ significantly. This

conclusion emphasizes the importance of using realistic channels and accurate characterization of UWB channels for system design and evaluation.

Bibliography

[1] M.-G. di Benedetto, T. Kaiser and N. Schmidt *UWB – State of the Art*, Journal of Applied Signal Processing Editorial, EURASIP publishing, March 2005.

[2] R. A. Scholtz, D. M. Pozar and W. Namgoong *Ultra-Wideband Radio*, Journal of Applied Signal Processing, EURASIP publishing, 2005:3, 252-272.

[3] U. S. Federal Communications Commission, FCC 02-48: First Report and Order.

[4] L. Yang and G. B. Giannakis,"Ultra-wideband communications," *IEEE Signal Process. Magazine*, vol. 21, no. 6, pp. 2654, Nov. 2004.

[5] A. F. Molisch *UWB Propagation Channels*, Book chapter 1, pp.1, 2005

[6] J. H. Reed et. al. *An Introduction to Ultra Wideband Communication Systems*, Prentice Hall, 2005.

[7] A. Batra, J. Balakrishnan, G. R. Aiello, J. R. Foerster and A. Dabak, "Design of a Multiband OFDM System for Realistic UWB Channel Environments", '*IEEE transactions on Microwave Theory and Techniques*, vol. 52, no. 9, Sept. 2004.

[8] M. G. Khan, A. A. Ashraf, J. Karedal, F. Tufvesson, and A. F. Molisch, "Measurements and Analysis of UWB Channels in Industrial Environments," *in Proc. Wireless Personal Multimedia Communications (WPMC)*, Aalborg, Denmark, Sept. 2005.

[9] A. Rajeswaran, V.S. Somayazulu, J. R. Foerster, "RAKE performance for a pulse based UWB system in a realistic UWB indoor channel," *Proc. IEEE International Conference on Communications (ICC '03)* , vol.4, pp. 2879 - 2883, 11-15 May 2003.

[10] B. Mielczarek, M. Wessman, and A. Svensson, "Performance of coherent UWB RAKE receivers with channel estimators," *Proc. IEEE Vehicular Technology Conference*, vol. 3, pp. 1880-1884, Oct. 2003.

[11] G. Durisi, S. Benedetto, "Performance of coherent and noncoherent receivers for UWB communications ," *Proc. IEEE International Conference on Communications (ICC 2004)*, vol. 6, pp. 3429-3433, June 20-24, 2004.

[12] S. Gezici, H. Kobayashi, H. V. Poor and A. F. Molisch, "Optimal and suboptimal linear receivers for time-hopping impulse radio systems," *Proc. IEEE Wireless Communications and Networking Conference (WCNC 2004)*, vol. 2, pp. 908-913, Atlanta, GA, March 2004.

[13] M. A. Rahman, S. Sasaki, Z. Jie, S. Muramatsu, H. Kikuchi, "Performance evaluation of RAKE reception of ultra wideband signals over multipath channels from energy capture perspective," *International Workshop on Ultra Wideband Systems, 2004. Joint with Conference on Ultrawideband Systems and Technologies,* pp. 231-235, May 2004.

[14] J. G. Proakis *Digital Communications*, 4th ed. Boston: McGraw-Hill, 2001.

[15] J. Karedal, S. Wyne, P. Almers, F. Tufvesson, and A. F. Molisch, "UWB channel measurements in an industrial environment", *in Proc. IEEE Globecom*, 2004.

[16] J. Karedal, S. Wyne, P. Almers, F. Tufvesson, and A. F. Molisch, "Statistical analysis of the UWB channel in an industrial environment," *in Proc. IEEE Vehicular Technology Conference*, 2004 fall.

[17] Y.-P. Nakache and A. F. Molisch, "Spectral shape of UWB signals influence of modulation format, multiple access scheme and pulse shape," *Proc. IEEE Vehicular Technology Conference, (VTC 2003-Spring)*, vol. 4, pp. 2510-2514, Jeju, Korea, April 2003.

[18] E. Fishler and H. V. Poor, "On the tradeoff between two types of processing gain," *Proceedings of the 40th Annual Allerton Conference on Communication, Control and Computing*, Monticello, IL, Oct. 2-4, 2002.

[19] A. F. Molisch et al., "IEEE 802.15.4a channel model - final report," Tech. Rep. Document IEEE 802.15-04-0662-02-004a, 2005.

[20] R. Qiu and I.-T. Lu, "Wideband wireless multipath channel modeling with path frequency dependence," *in IEEE International Conference on Communications (ICC96)*, 1996.

[21] R. C. Qiu and I. Lu, "Multipath resolving with frequency dependence for broadband wireless channel modeling," *IEEE Trans.Veh. Tech., 1999.*

[22] T. S. Rappaport, *Wireless Communications: Principles and Practice*, Prentice Hall PTR, Upper Saddle River, NJ, USA, 2nd edition, 2002.

[23] A. Saleh and R. Valenzuela, "A statistical model for indoor multipath propagation," *IEEE Journal on Select. Areas Commun.*, vol. SAC-5, no. 2, pp. 128-137, Feb. 1987.

[24] D. Cassioli, M. Z.Win, F. Vatalaro, and A. F. Molisch, "Performance of low-complexity Rake reception in a realistic UWB channel," *Proc. IEEE ICC'03*, vol.2, pp.763767, 2003.

[25] D. J. Choi and W. E. Stark, "Performance of ultra-wideband communications with suboptimal receivers in multipath channels," *IEEE Journal of Sleceted Areas Comm.*, vol. 20, no. 9, Dec. 2002, 1754-1766.

[26] A. F. Molisch et al., "An efficient low-cost time-hopping impulse radio for high data rate transmission," *Proc. IEEE 6th International Symposium on Wireless Personal Multimedia Communications (WPMC 2003)*, Yokosuka, Kanagawa, Japan, Oct. 19-22, 2003.

[27] S. Gezici, H. Kobayashi, H. V. Poor and A. F. Molisch, "Performance evaluation of impulse radio UWB systems with pulse-based polarity randomization in asynchronous multiuser environments," *Proc. IEEE Conference on Ultra Wideband Systems and Technologies (UWBST 2004)*, Kyoto, Japan, May 18-21, 2004.

[28] F. Rajwani, N.C. Beaulieu, "Simplified bit error rate analysis of PAPM-UWB with MRC and EGC in lognormal fading channel," *Proc. IEEE ICC'05*, vol. 5, pp. 2886-2889, May 2005.

[29] J.R. Foerster, "The effects of multipath interference on the performance of UWB systems in an indoor wireless channel," *in Proc. IEEE Vehicular Technology Conf.*, Rhodes, Greece, May, 2001, pp. 1176-1180.